et al., 2005). It is known that oxygen is initially converted to superoxide anion (O_2^-), one of several reactive oxygen species (ROS), by electron leakage. This occurs primarily from complex III of the electron transport system present in mitochondria and constitutes the major endogenous source of ROS (Turrens *et al.*, 1985; Lenaz, 1998; Finkel and Holbrook, 2000; Raha, and Robinson, 2000). Such endogenously generated ROS readily attack a wide variety of cellular entities, resulting in damage that compromises cell integrity and function (Vuillaume, 1987; Collins *et al*, 1997). We found that the *Rhei Rhizoma* has a role of anti-oxidant, which suppress O_2^- generation from mitochondria and extends the life span of *C. elegans*.

Materials and Methods

1. Materials

C. elegans, wild-type and a *fer-15* (*hc15*) mutant strain were obtained from the Caenorhabditis Genetics Center, University of Minnesota. Animals were cultured on nematode growth medium (NGM) agar plates seeded with the *Escherichia coli* (*E. coli*) strain OP50 at 20°C as previously described (Brenner, 1974). Embryos (eggs) were collected from young adult hermaphrodite on NGM agar plates using alkaline sodium hypochlorite (Emmons *et al.*, 1979). The released eggs were allowed to hatch by overnight incubation at 20°C in S basal buffer [100 mM NaCl, 50 mM potassium phosphate (pH 6.0)] (Sulston and Brenner, 1974).

Kampo medicines: *daisaikoto, shosaikoto, saikokeishito, orengedokuto, tokishakuyakusan, keishibukuryogan, shigyakusan, hochuekkito, rikkunshito, shichimotsukokato, chotosan, juzentaihoto, seihaito, daikenchuto, goshajinkigan, saireito.*

Crude drugs: *Paeoniae Radix, Cinnamomi Cortex, Moutan Cortex, Glycyrrhizae Radix, Ginseng Radix, Zingiberis Rhizoma, Bupleuri Radix, Scutellariae Radix, Rhei Rhizoma, Ephedrae Herba.*

These Kampo medicines and crude drugs were kindly provided by the Tsumura Company.

2. Measurement of life span

NGM agar medium plates seeded with the *E. coli* strain OP50 as already described (Honda *et al.*, 1993; Adachi *et al.*, 1998; Ishii *et al.*, 1998) were used for both growth and determination of the life spans of wild-type and *fer-15* mutant hermaphrodites. 5-fluoro-2'-deoxyuridine (FudR) has been used after maturation in order to prevent the progeny production of wild type on NGM agar plate (Mitchell *et at.*, 1979). S medium (Sulston and Brenner, 1974) containing Bacto-peptone of various concentrations (a standard concentration was 2.5 g Bacto-peptone in 1,000 ml of the medium: x1) seeded with the *E. coli* strain OP50 was used to determine the life spans of the *fer-15* mutant in liquid medium. *E. coli* strain OP50 was cultured in 500 ml of LB medium [10 g Bacto-tryptone, 5 g yeast extract, 10 g NaCl, pH 7.0] at 37°C over night. After centrifugation at 3,000 rpm for 15 min, the pellet was suspended in 500 ml of the S medium. About 2,000 newly hatched larvae (L1-stage larvae) were added in 10 ml of the S medium into a 50 ml conical flask and incubated at 25°C for 100 rpm in a shaker (ISF-1-W, Kühner SHAKER, Switzerland). It was possible that some test samples inhibited *E. coli* growth, thereby affecting *C. elegans* life spans. In order to avoid this, a final concentration of 200 μg/ml of ampicillin was added in the S medium after animals reached to adulthood (4 days after the L1 stage-larvae were added in the S medium) in order to inhibit the *E. coli* proliferation. To measure life span, the numbers of living and dead animals in 300 μl of the medium in each flask were counted every few days.

3. Measurement of body size

Body length and width of animals from L1 stage to adult stage were measured daily during the six days after hatching.

4. Isolation of mitochondria

L4-stage wild-type animals were employed for mitochondrial isolation. A flotation method was used to remove debris and dead animals from living animals (Lewis *et al*, 1995). In brief, NGM agar plates were washed and the contents were suspended in ice-cold S basal buffer and mixed with an equal volume of ice-cold 60% sucrose. After centrifugation for 15 second at 3,000 rpm, the floating animals were transferred to a fresh tube. They were washed three times with S basal buffer and once with isolation buffer (210 mM mannitol, 70 mM sucrose, 0.1 mM EDTA and 5 mM Tris-HCl, pH 7.4). The animals were homogenized in isolation buffer using a teflon homogenizer. The debris was removed by a differential centrifugation at 600 x *g*. The supernatant was then centrifuged at 7,200 x *g* and the mitochon-

dria-containing pellet was suspended in TE buffer [50 mM Tris-HCl (pH 7.4), 0.1 mM EDTA]. Sub-mitochondrial particles (SMP) were employed in these experiments because they are known to be depleted in the mitochondrial superoxide dismutase that transforms superoxide anion to hydrogen peroxide. SMP were obtained by sonicating freeze-thawed mitochondria twice for 20 s separated by 1 min intervals in a model U200S sonicator (IKA Labortechnik). SMP were washed twice at isolation buffer and suspend in TE buffer.

5. Measurement of superoxide anion (O_2^-)

O_2^- production was measured using the chemiluminescent probe MPEC (2-methyl-6-p-methoxyphenylethynyl-imidazopyrazinone) (ATTO Co., Tokyo, Japan)(Shimomura *et al.*, 1998; Yasuda *et al.*, 2006). MPEC has an advantage of low background relative to MCLA (3,7-dihydro-2-methyl-6- (4-methoxyphenol) imidazol [1,2-a]pyrazin-3-one) that is generally used. 5 μg of SMP was added to 1 ml of assay buffer (50 mM HEPES-NaOH, pH 7.4, 2 mM EDTA) containing 0.7 μM MPEC. 5 μg/ml of *Rhei Rhizoma* was added in the SMP solution, which was placed into a photon counter with an AB-2200 type Luminescencer-PSN (ATTO Co., Tokyo, Japan) and measured at 37°C. The rates of O_2^- were expressed as counts per second.

6. Statistical analysis

Statistical analysis was carried out by Student's *t* test and Tukey's multiple-range test.

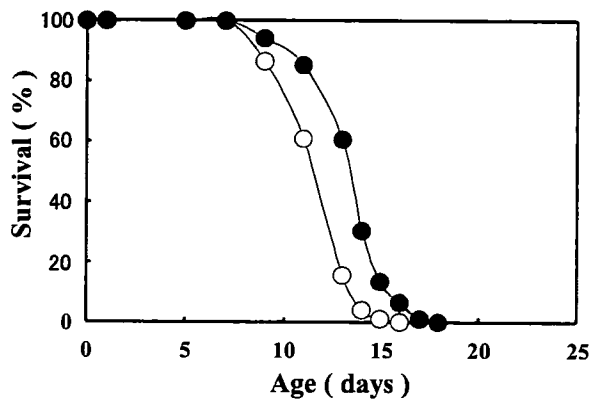

Fig. 2. Life spans of wild type N2 (closed circles) and a *fer-15* mutant (open circles) grown on NGM agar plates. 100 animals were measured for each strain at 25°C.

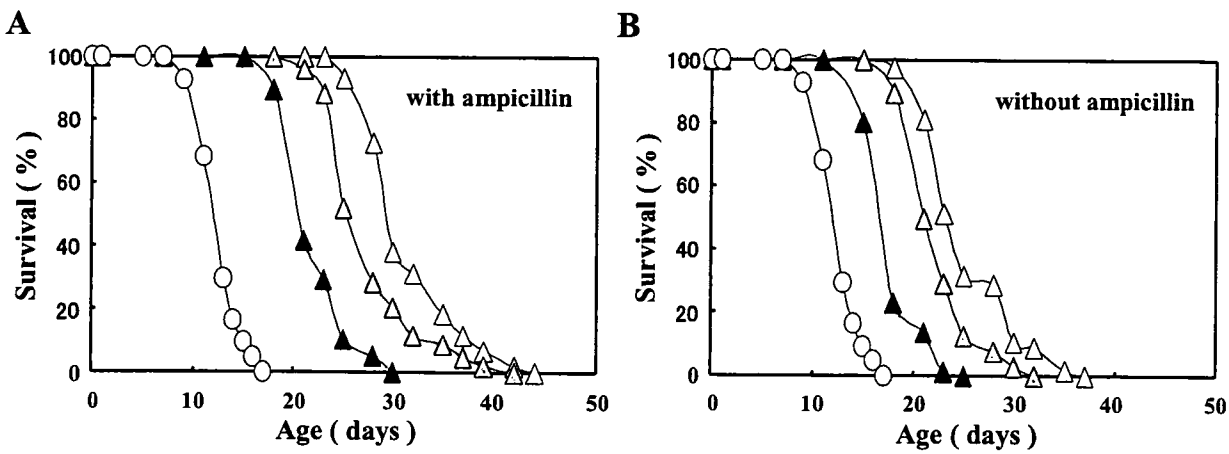

Fig. 3. Life spans of a *fer-15* mutant grown on NGM agar plate and in S medium containing various concentrations of Bacto-peptone with (A) and without ampicillin (B). Open circles: on NGM agar plates; open triangles: with a standard concentration of Bacto-peptone in liquid medium; ashen triangle: two-fold Bacto-peptone; closed triangles, four-fold Bacto-peptone. 100 animals were measured from the NGM agar plates. See also Table 1.

Results and Discussion

1. Development of the system

To develop a low cost and quick assay system using the free-living nematode, *Caenorhabditis elegans* (*C. elegans*) for identifying Kampo medicines and crude drugs with macrobiotic activity, a suitable assay was designed and tested. The life span of a *fer-15* mutant was slightly shorter than the wild type N2 on NGM agar plate (Fig. 2). The life spans decreased depending on the concentration of Bacto-peptone in the S medium (Fig. 3A; Table 1). The presence of ampicillin contributed to extend life span (Fig. 3B; Table 1), suggesting that caloric restriction to adult animals resulted in the extension of life span. Concentrations of Bacto-peptone in the S medium contributed markedly to body width but slightly to body length (Fig. 4A and 4B; Table 2A and 2B), suggested that the diet from *E. coli* affected to life span and body size. A four-fold concentration of Bacto-peptone in S medium gave the same body size of *C. elegans* adults as those grown on NGM agar plats (Fig. 4A and 4B; Table 2A and 2B.). In even Bacto-peptone of the standard concentration in S medium, animals appeared to be healthy.

In recent years, anti-aging studies for our health and longevity have been the subject of intense interest and experimentation. Physiologically functional nutrition as well as basic nutrition are especially studied. Our system has the potential to assist in identifying undiscovered natural endowments or chemicals with macrobiotic activities. We provide an example of this below.

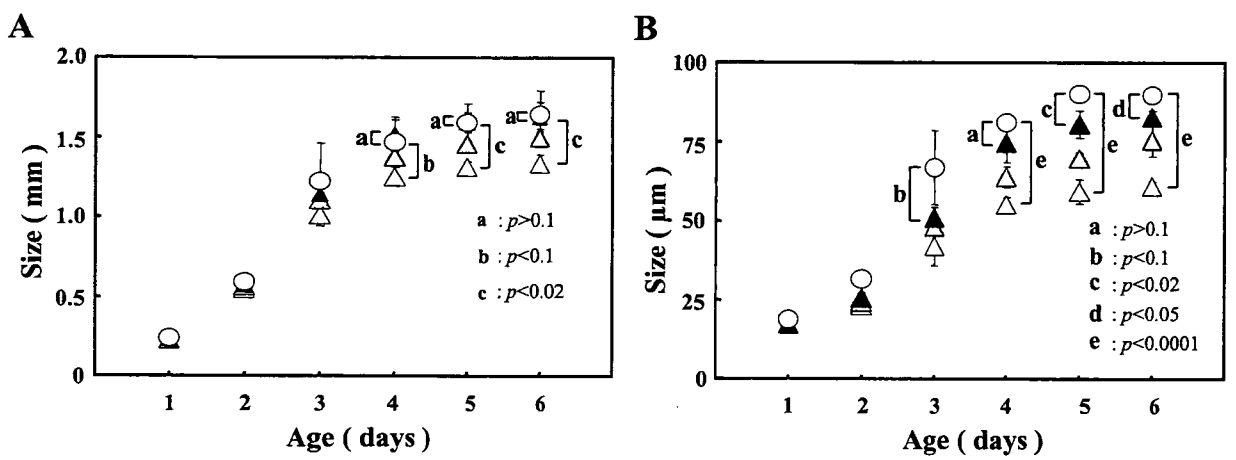

Fig. 4. Mean body length (A) and width (B) at different days of development. Open circles: on NGM agar plate; open triangles: with a standard concentration of Bacto-peptone in S medium; ashen triangles: two-fold Bacto-peptone; closed triangles, four-fold Bacto-peptone. Each symbol with error bars indicates the mean values with the standard deviations from three separate experiments. 25 animals were measured at each point in each experiment. See also Table 2.

Table 1. Life spans (mean and maximum life spans ± standard deviation) of the *fer-15* mutant grown on NGM agar plates and in S medium containing various concentrations of Bacto-peptone with and without ampicillin. Each value indicates the mean of three separate experiments.

Concentrations of Bacto-Peptone in S medium	Ampicillin	Life span (days)	
		Mean life span	Maximum life span
x 1	+	30.5 ± 2.02	40.3 ± 4.04
x 1	-	24.1 ± 2.77	32.7± 5.14
x 2	+	26.9 ± 1.62	36.7± 5.03
x 2	-	21.7 ± 2.48	29.7± 4.04
x 4	+	21.1 ± 1.93	27.7± 2.52
x 4	-	17.4 ± 1.62	22.7± 2.52
On NGM medium	-	12.5 ± 0.31	16.3 ± 0.58

2. The longevity effects of Kampo medicines and crude drugs

As a preliminary study, the life spans of the 16 Kampo medicines and 10 crude drugs were examined in S medium containing Bacto-peptone of a standard concentration and ampicillin. In these medicines and drugs, 8 different Kampo medicines (*daisaikoto*, *syosaikoto*, *saikokeishito*, *tokishakuyakusan*, *keishibukuryogan*, *shigyakusan*, *shichimotsukokato* and *daikenchuto*) and 3 crude drugs (*Moutan Cortex*, *Ginseng Radix* and *Bupleuri Radix*) had no effect on *C. elegans* life span in the S medium even at high concentrations (Fig. 5A, Table 3A and 3B). Figure 5A showed the result of *saikokeishito* as an example of this. On the other hand, 6 Kampo medicines (*orengedokuto*, *hochuekkito*, *rikkunshito*, *juzentaihoto*, *seihaito*, and *saireito*) and 6 crude drugs (*Paeoniae Radix*, *Cinnamomi Cortex*, *Glycyrrhizae Radix*, *Zingiberis Rhizoma*, *Scutellariae Radix* and *Ephedrae Herba*) shortened the life span (Fig. 5B, Table 3A and 3B). Figure 5B showed the result using *saireito*. The crude drugs possessed a greater likelihood of decreasing life span. While the reason for the life shorting effect is still unknown, these drugs may have cytotoxicity through a variety of mechanisms, including anti-bacterial, anti-viral, detoxication or

Table 2. Growth rates of body length (A) and body width (B) of the *fer-15* mutant on NGM agar plates or in S medium containing a standard concentration of Bacto-peptone. Each value indicates the mean of three separate experiments. Approximately 25 animals were used in each experiment. Statistic comparisons of body length and width values between on NGN agar plate and in S medium were determined.

A. Body length (mm)

Concentrations of Bacto-Peptone in S medium	Days					
	1	2	3	4	5	6
x 1	0.23 ± 0.01	0.50 ± 0.01	1.01 ± 0.07	1.25 ± 0.06	1.31 ± 0.03	1.33 ± 0.06
x 2	0.23 ± 0.01	0.57 ± 0.02	1.11 ± 0.05	1.37 ± 0.04	1.46 ± 0.02	1.49 ± 0.06
x 4	0.23 ± 0.01	0.57 ± 0.02	1.14 ± 0.05	1.52 ± 0.09	1.59 ± 0.06	1.63 ± 0.09
On NGM medium	0.24 ± 0.02	0.59 ± 0.03	1.22 ± 1.47	1.47 ± 0.16	1.59 ± 0.12	1.64 ± 0.15

B. Body width (μm)

Concentrations of Bacto-Peptone in S medium	Days					
	1	2	3	4	5	6
x 1	17 ± 1	23 ± 2	42 ± 6	55 ± 2	59 ± 4	61 ± 2
x 2	17 ± 1	24 ± 2	48 ± 3	64 ± 3	69 ± 1	76 ± 5
x 4	17 ± 1	26 ± 2	51 ± 3	75 ± 6	81 ± 4	83 ± 2
On NGM medium	19 ± 2	32 ± 2	67 ± 12	81 ± 2	89 ± 2	89 ± 1

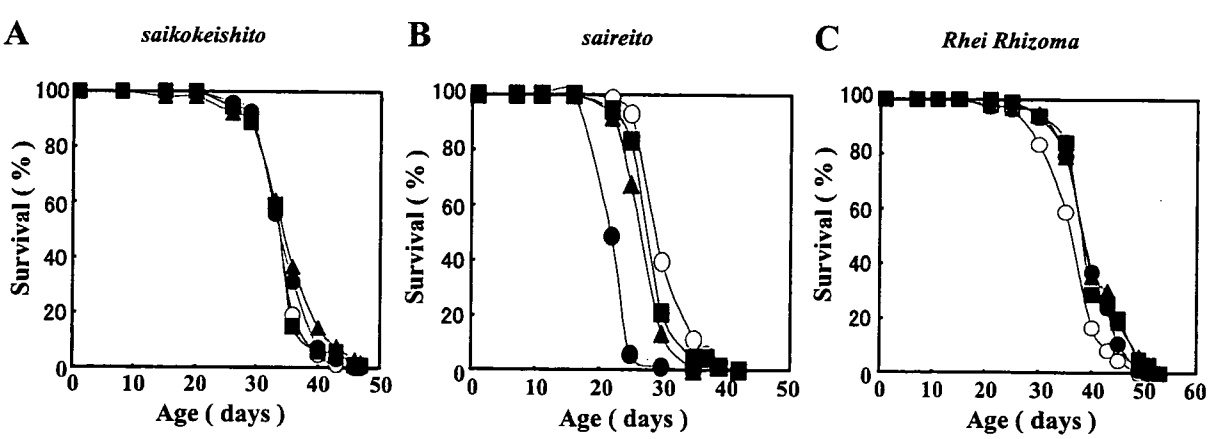

Fig 5. Life spans of a *fer-15* mutant in various kinds and concentrations of some Kampo medicines and crude drugs in S medium containing a standard concentration of Bacto-peptone. Open circles: control; Closed circles: 500 μg/ml; closed triangles: 100 μg/ml; closed squares 50 μg/ml.

Table 3. Effects of Kampo medicines (A) and crude drugs (B) on mean and maximum life spans of the *fer-15* mutant in S medium containing a standard concentration of Bacto-peptone. Effect showed effect on life span in each concentration of samples compared to control: -: shorter; ±: same ; +: longer. Statistic comparisons of mean life-span values between control and sample were determined by Tukey's multiple-range test.

A. Life spans in Kampo medicines

Name	Conc (μg/ml)	Median Life-span (days)	Maximum Life-span (days)	*p* value	Effect
daisaikoto	0	31.1	39		
	500	31.6	42	< 0.1	±
syosaikoto	0	31.1	39		
	500	32.3	44	< 0.1	±
saikokeishito	0	35.2	46		
	500	35.8	46	< 0.1	±
	100	36.2	48	< 0.1	±
	50	35.1	48	< 0.1	±
orengedokuto	0	35.2	46		
	500	30.5	40	<0.001	-
	100	33.1	46	<0.001	-
	50	33.9	46	< 0.05	-
tokishakuyakusan	0	31.3	39		
	500	30.4	39	< 0.1	±
keishibukuryogan	0	31.3	39		
	500	31.8	42	< 0.1	±
shigyakusan	0	31.3	39		
	500	32.8	43	< 0.1	±
hochuekkito	0	35.2	46		
	500	31.7	43	<0.001	-
	100	34.2	46	< 0.1	±
	50	34.1	46	< 0.1	±
rikkunshito	0	35.2	46		
	500	30.1	39	<0.001	-
	100	30.1	46	<0.001	-
	50	33.4	46	<0.005	-
shichimotsukokato	0	36.1	46		
	500	36.5	49	< 0.1	±
	100	35.1	45	< 0.1	±
	50	35.3	45	< 0.1	±
chotosan	0	36.1	46		
	500	38.0	49	<0.005	+
	100	35.8	49	< 0.1	±
	50	35.9	49	< 0.1	±
juzentaihoto	0	37.1	46		
	500	35.9	45	< 0.1	-
	100	34.6	46	< 0.05	-
	50	34.6	45	< 0.02	-
seihaito	0	36.1	46		
	500	30.0	42	<0.001	-
	100	34.5	45	< 0.02	-
	50	34.6	45	< 0.05	
daikenchuto	0	36.1	46		
	500	35.4	46	< 0.1	±
	100	36.1	45	< 0.1	±
	50	34.9	45	< 0.1	±
goshajinkigan	0	31.9	42		
	500	30.7	37	<0.005	-
	100	34.1	46	<0.002	+
	50	32.1	39	< 0.1	±
saireito	0	31.9	42		
	500	23.8	35	<0.001	-
	100	28.8	35	<0.001	-
	50	30.3	42	< 0.01	-

defervescence. Of the 26 medicines, high concentrations of *chotosan*, which is employed to treat headaches, and *Rhei Rhizoma*, which has stomach and laxative properties, expanded the life span of *C. elegans* (Fig. 5C, Table 3A and 3B). The goshajinkigan, which is employed to achieve reversal of weak physical condition in elderly people, extended the life span at a concentration of 100 μg/ml, but reduced it at 500 μg/ml. Figure 5C shows the results using *Rhei Rhizoma. Rhei*

Table 3 B. Life spans in crude drugs

Name	Conc. (μg/ml)	Median Life-span (days)	Maximum Life-span (days)	*p* value	Effect
Paeoniae Radix	0	32.9	39		
	500	29.7	35	<0.001	-
	100	31.9	37	< 0.1	±
	50	30.1	42	<0.01	-
Cinnamomi Cortex	0	31.9	39		
	500	21.9	44	<0.001	-
	100	28.1	37	<0.001	-
	50	27.2	39	<0.001	-
Moutan Cortex	0	35.2	47		
	500	28.4	39	<0.001	±
	100	-	-	-	
	50	32.7	47	<0.001	±
Glycyrrhizae Radix	0	35.2	47		
	500	-	-	-	-
	100	34.5	47	< 0.1	-
	50	35.0	42	< 0.1	-
Ginseng Radix	0	37.7	49		
	500	38.4	45	< 0.1	±
	100	38.4	51	< 0.1	±
	50	38.2	49	< 0.1	±
Rhei Rhizoma	0	31.2	39		
	500	33.2	45	< 0.02	+
	100	35.4	43	<0.001	+
	50	34.1	43	<0.001	+
Rhei Rhizoma	0	37.7	49		
	500	40.6	51	<0.001	+
	100	41.0	53	<0.001	+
	50	41.2	53	<0.001	+

Name	Conc. (μg/ml)	Median Life-span (days)	Maximum Life-span (days)	*p* value	Effect
Zingiberis Rhizoma	0	38.4	49		
	500	29.7	45	<0.001	-
	100	34.3	49	<0.001	-
	50	37.6	51	< 0.1	±
Bupleuri Radix	0	38.4	49		
	500	26.9	42	<0.001	±
	100	36.1	51	<0.001	±
	50	35.5	51	<0.001	±
Scutellariae Radix	0	38.4	49		
	500	22.3	30	<0.001	-
	100	23.3	30	<0.001	-
	50	30.1	45	<0.001	-
Ephedrae Herba	0	34.8	42		
	500	29.6	35	<0.001	-
	100	35.3	44	< 0.1	±
	50	34.3	44	< 0.1	±

Rhizoma in a four-fold concentration of Bacto-peptone in S medium as well as a standard concentration of Bacto-pepton also expanded the life span of *C. elegans* (data not shown). This suggests that the effect on life span is not dependent on concentration of Bacto-peptone.

3. Rhei Rhizoma is an antioxidant

Recently, much attention has been focused on the hypothesis that oxidative damage plays a role in cellular and organismal aging. It is known that some anti-oxidants expand life span of *C. elegans* (Melov *et al*, 2000; Ishii *et al*, 2004). We examined the suppressive effects of mitochondrial O_2^- by *Rhei Rhizoma*, one of the life-span enhancing medicines, to determine if the life-span extension was due to its antioxidant properties. In fact, *Rhei Rhizoma* decreased O_2^- levels, suggested that this crude drug has anti-oxidant ability (Fig. 6). We hope to isolate a single component with longevity effect from *Rhei Rhizoma* extracts using the life-span testing system described above. As *C. elegans* holds the distinction of being the first metazoan to have its genome completely sequenced and all of genes are identified (The *C. elegans* Sequencing Consortium, 1988), exam-

ining gene expression using DNA microarrays will allow us to elucidate the life-span promoting mechanism of *Rhei Rhizoma* at the molecular level.

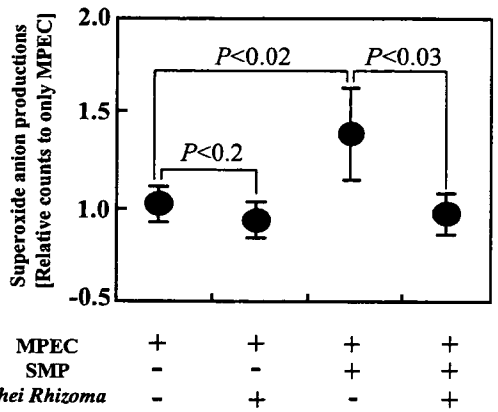

Fig. 6. Superoxide anion production. Each column with error bars indicates the mean value with the standard deviation from three separate experiments.

Acknowledgements

This work is supported by grant-in-aid for Aging Research from the Ministry of Health, Labor and Welfare, Japan.

References

Adachi, H., Fujiwara,Y., and Ishii, N. (1998) Effects of oxygen on protein carbonyl and aging in *Caenorhabditis elegans* mutants with long (*age-1*) and short (*mev-1*) life spans, *J. Geront.: Biol. Sc.i*,, 53, B240-B244.

Brenner, S. (1974) The genetics of *Caenorhabditis elegans*, *Genetics*, 77, 71-94.

Collins, A.R., Duthie, S.J., Pillion, L., Gedik, C.M., Vaughan, N., and Wood, S.G. (1997) Oxidative DNA damage in human cells: The influence of antioxidants and DNA repair, *Biochem. Soc. Transact.*, 25, 326-331.

Emmons, S.W., Klass, M.R., and Hirsh, D. (1979) Analysis of the constancy of DNA sequenced during development and evolution of the nematode *Caenorhabditis elegans*, *Proc. Natl. Acad. Sci. USA*, 76, 1333-1337.

Finkel, T., and Holbrook, N. J. (2000) Oxidants, oxidative stress and the biology of ageing, *Nature*, 408, 239-247.

Haenold, R., Wassef, D.M., Heinemann, S.H., and Hoshi, T. (2005) Oxidative damage, aging and anti-aging strategies, *Age*, 27, 183-199.

Honda, S., Ishii, N., Suzuki, K. and Matsuo, M. (1993) Oxygen-dependent perturbation of life span and aging rate in the nematode, *J. Geront.: Biol. Sc.i*, 48, B57-B61.

Hosokawa, H., Ishii, N., Ishida, H., Ichimori, K., Nakazawa, H., and Suzuki, K. (1994) Rapid accumulation of fluorescent material with aging in an oxygen-sensitive mutant *mev-1* of *Caenorhabditis elegans*, *Mech. Ageing Dev.*, 74, 161-170.

Houthoofd, K., Braeckman, B.P., Lenaerts, I., Brys, K., De Vreese, A., Van Eygen, S., and Vanfleteren, J.R. (2002) No reduction of metabolic rate in food restricted *Caenorhabditis elegans*, *Exp. Geront.*, 37, 1357-1367.

Ishii, N., Fujii, M., Hartman, P.S., Tsuda, M., Yasuda, K., Senoo-Matsuda, N., Yanase, S., Ayusawa, D., and Suzuki, K. (1998) A mutation in succinate dehydrogenase cytochrome *b* causes oxidative stress and ageing in nematodes, *Nature*, 394, 6694-6697.

Ishii, N., Goto, S., and Hartman, P.S. (2002) Protein oxidation during aging of the nematode *Caenorhabditis elegans*, *Free Radic. Biol. Med.*, 33, 1021-1025.

Ishii, N., Senoo-Matsuda, N., Miyake, K., Yasuda, K., Ishii, T., Hartman, P.S., and Furukawa, S. (2004) Coenzyme Q_{10} can prolong *C. elegans* lifespan by lowering oxidative stress, *Mech. Ageing Dev.*, 125, 41-46.

Jansson, H.B., Jeyaprakash, A., Marban-Mendoza, N., and Zuckerman, B.M. (1986) *Caenorhabditis elegans*: comparisons of chemotactic behavior from monoxenic and axenic culture, *Exp. Parasitol.*, 61, 369-372.

Jewitt, N., Anthony, P., Lowe, K.C., and De Pomerai, D.I. (1999) Oxygenated perfluorocarbon promotes nematode growth and stress-sensitivity in a two-phase liquid culture system, *Enzyme Microbial. Tech*, 25, 349-356.

Kishikawa, M., and Sakae, M. (1997) Herbal medi-

cine and the study of aging in senescence-accelerated mice (SAMP1TA/Ngs), *Exp. Geront.*, 32, 229-242.

Klass, M. (1977) Aging in the nematode *Caenorhabditis elegans*: Major biological and envieonmental factors influencing life span, *Mech. Ageing Dev.*, 6, 413-429.

Klass, M., and Hirsh, D. (1976) Non-ageing developmental variant of *Caenorhabditis elegans*, *Nature*, 260, 523-525.

Lenaz, G., (1998) Role of mitochondria in oxidative stress and ageing, *Biochim. Biophys. Acta.*, 1366, 53-67.

Lewis J.A., and Fleming. J.T. (1995) Basic culture method: Modern Biological Analysis of an Organism: Method in Cell Biology, eds. by H. F. Epstein and D.C. Ashakes, pp.3-29, Academic Press U.K.

Luo, Y. (2006) Alzheimer's disease, the nematode *Caenorhabditis elegans*, and ginkgo biloba leaf extract, *Life Sci.*, 78, 2066-2072.

Melov, S., Ravenscroft, J., Malik, S., Gill, M.S., Waker, D.W., Clayton, P.E., Wallace, D.C., Malfroy, B., Doctrow, S.R., and Lithgow, G.J. (2000) Extension of life-span with superoxide dismutase/catalase mimietics, *Science*, 289, 1567-1569.

Mitchell, D.H., Stiles, J.W., Santelli, J., and Rad Sanadi, D. (1979) Synchronous growth and aging of *Caenorhabditis elegans* in the presence of fluorodeoxyuridine, *J. Geront.*, 35, 28-36.

Petrascheck, M., Ye, X. and Buck, L.B. (2007) An antidepressant that extends lifespan in adult *Caenorhabditis elegans*, *Nature*, 450, 553-556.

Raha, S., and Robinson, B. H. (2000) Mitochondria, oxygen free radicals, disease and ageing, *Trends Biochem. Sci*,, 25, 502-508.

Roberts, T.M., and Ward, S. (1982) Membrane flow during nematode spermigenesis, *J. Cell Biol.*, 92, 113-120.

Shimomura, O., Wu, C., Murai, A., and Nakamura, H. (1998) Evaluation of five imidazopyrazinone-type chemiluminescent superoxide probes and their application to the measurement of superoxide anion generated by Listeria monocytogenes, *Anal. Biochem.*, 258, 230-235.

Sulston J.E., and Brenner S. (1974) The DNA of *Caenorhabditis elegans*, *Genetics*, 77, 95-104.

Sulston, J.E. (1988) Cell lineage. in The nematode *Caenorhabditis elelgans*, ed. by W. B. Wood, pp.123-155, Cold Spring Harbor Laboratory N.Y.

Sulston, J.E., and Horvitz, H.R. (1977) Post-embryonic cell lineages of the nematode *Caenorhabditis elegans*, *Dev. Biol.*, 56, 110-156.

The C. elegans Sequencing Consortium. (1988) Genome sequence of the nematode *C. elegans*: a platform for investigating biology, *Science*, 282, 2012–2018.

Turrens, J.F., Alexandre, A., and Lehninger, A.L. (1985) Ubisemiquinone is the electron donor for superoxide formation by complex III of heart mitochondria, *Arch. Biochem. Biophys.*, 237, 408-414.

Vanfleteren, J.R. (1980) Nematods as nutritional models. in Nematodes as biological models, Volume 2: Aging and other model systems, ed. by B. M. Zuckerman, pp.47-49, Academic Press N.Y.

Vuillaume, M. (1987) Reduced oxygen species, mutation, induction and cancer initiation, *Mutat. Res.*, 186, 43-72.

Wood, W.B., (1988) Embryology, in The nematode *Caenorhabditis elelgans*, by W. B. Wood, pp. 215-241, Cold Spring Harbor Laboratory N.Y.

Yasuda, K., Ishii, T., Suda, H., Akatsuka, A., Hartman, P.S., Goto, S., Miyazawa, M., and Ishii, N. (2006) Age-related changes of mitochondrial structure and function in *Caenorhabditis elegans*, *Mech. Ageing Dev.*, 127, 763-770.

Corresponding author:
Naoaki Ishii
Department of Molecular Life Science
Tokai University School of Medicine
143 Shimokasuya, Isehara, Kanagawa 259-1193
Japan
Tel: +81-463-93-1121x2651
Fax: +81-463-94-8884
E-mail: nishii@is.icc.u-tokai.ac.jp

European Journal of Neurology 2007, 14: 1029–1034 doi:10.1111/j.1468-1331.2007.01870.x

Clinical and experimental features of MuSK antibody positive MG in Japan

K. Ohta[a], K. Shigemoto[b], A. Fujinami[c], N. Maruyama[d], T. Konishi[e] and M. Ohta[a,c]

[a]*Clinical Research Center, Utano National Hospital, Kyoto, Japan;* [b]*Department of Preventive Medicine, Faculty of Medicine, Graduate School of Ehime University, Ehime, Japan;* [c]*Department of Medical Biochemistry, Kobe Pharmaceutical University, Kobe, Japan;* [d]*Tokyo Metropolitan Institute of Gerontology, Tokyo, Japan; and* [e]*Department of Neurology, Utano National Hospital, Kyoto, Japan*

Keywords:
clinical features, domain, IgG subclass, muscle specific tyrosine kinase, MuSK antibody, myasthenia gravis, seronegative myasthenia gravis

Received 28 December 2006
Accepted 7 May 2007

We investigated the presence of antibodies (Abs) against muscle-specific tyrosine kinase (MuSK) in Japanese myasthenia gravis (MG) patients. MuSK Abs were found in 23 (27%) of 85 generalized seronegative MG (SNMG) patients but not in any of the ocular MG patients. MuSK Ab-positive patients were characterized as having female dominance (M:F, 5:18), age range at onset 18 to 72 (median 45) years old, and prominent oculobulbar symptoms (100%) with neck (57%) or respiratory (35%) muscle weakness. Limb muscle weakness was comparatively less severe (52%), thymoma absent. Most patients had good responses to simple plasma exchange and steroid therapy. MuSK IgG from all 18 patients was exclusively the IgG 4 subclass and bound mainly with the MuSK Ig 1–2 domain. Serial studies of 12 individuals showed a close correlation between the variation in MuSK Ab titers and MG clinical severity ($P = 0.01$ by Kruskal–Wallis). MuSK Ab titers were sharply decreased in patients who had a good response to early steroid therapy or simple plasma exchange, but there was no change, or a rapid increase on exacerbation after thymectomy. Measurement of MuSK Ab titers aids in the diagnosis of MG and the monitoring of clinical courses after treatment.

Introduction

Muscular weakness in most patients with myasthenia gravis (MG) is caused by an antibody (Ab)-mediated autoimmune response to muscle nicotinic acetylcholine receptors (AChRs), but there is no correlation between the AChR Ab level and degree of muscle weakness. This may be because of AChR Abs heterogeneity and epitope specificity or the presence of Abs against other functionally important muscle antigens. Fifteen percent of patients with generalized MG who have no detectable circulating Abs to AChR are termed seronegative MG (SNMG). Autoantibodies against muscle-specific tyrosine kinase (MuSK) have been identified in that population [1]. The positivity for MuSK Ab in SNMG patients varied from 3.8% to 71% by studies [1–11], which may be due to geographical or ethnic differences. Immunoglobulin allotypes in Caucasian and Chinese MG patients differ from those in Japanese patients [12]. We performed a MuSK Ab survey of a large number of Japanese MG patients and characterized the clinical features of those who were MuSK Ab positive. Furthermore, we investigated the correlation between MuSK Ab titer and disease severity, epitope specificity, and the IgG subclass of MuSK IgG.

Correspondence: Mitsuhiro Ohta, Department of Medical Biochemistry, Kobe Pharmaceutical University, Motoyamakita, Higashinada-ku, Kobe 658–8558, Japan (tel.: +81 78 441 7557; fax: +81 78 441 7559; e-mail: mohta@kobepharma-u.ac.jp).

Patients and methods

Patients

We studied 85 patients (27 men, 58 women, mean age 56 years old, range 18–76 years) who had generalized SNMG and were consistently negative for serum AChR Abs, as well as 272 AChR Ab-positive MG (SPMG) patients (87 men, 185 women, mean age 54 years old; age range 32–74 years); 50 with and 222 without thymoma. The control populations comprised 70 healthy participants (29 men, 41 women; mean age 50 years old, range 27–74 years) and 91 patients (37 men, 54 women; mean age 50 years old, range 32–74 years) with other neurological or immunological diseases (five Lambert-Eaton myasthenic syndrome, six polymyositis, 10 muscular dystrophy, 15 thyroiditis, 10 type 1 diabetes mellitus, five rheumatoid arthritis, 10 multiple sclerosis, five spinal progressive muscular atrophy, five chronic inflammatory demyelinating polyneuropathy, 10 amyotrophic lateral sclerosis, and 10 epilepsy). The study was approved by the ethics committee of Utano National Hospital. All persons gave their informed consent prior to their inclusion in the study.

Preparation of recombinant human MuSK protein

To produce his-tag human MuSK protein, the entire extracellular domain (MuSK 1–4; nucleotides 107–1526,

GenBank/EMBL accession number AF006464) of human MuSK, and MuSK fragments comprised of the first half bearing two Ig-domains (MuSK 1–2; nucleotides 107–700) were linked to the PCR3.1/Myc-His vector (Invitrogen Corporation, Carlsbad, CA, USA) [13]. Membrane-proximal extracellular domains, including Ig-domains 3 and 4 (MuSK 3–4; nucleotides 701–1526), were linked to the pSecTag-His vector (Invitrogen) carrying the ER signal sequence of the mouse Igκ gene. All constructs were transiently transfected to COS7 cells [14]. The recombinant his-tag MuSK secreted was purified in a histidine-affinity column (Clonetech Laboratories, Palo Alto, CA, USA). Recombinant protein purity was determined by SDS-PAGE with silver staining. Recombinant protein concentrations were obtained with a BCA Protein assay kit (Pierce, Biotechnology, Inc., Rockfold, IL, USA) with bovine serum albumin as the standard. The MuSK extracellular domain and MuSK fragments then were labeled with ^{125}I [15].

Detection of MuSK Ab by radioimmunoprecipitation assay

All the sera underwent a radioimmunoassay (RIA) to determine the presence of MuSK Ab. In brief, 5 μl of each sample was incubated overnight at 4°C with 50 μl of ^{125}I-his-tag MuSK (40 000 cpm), after which 50 μl of anti-human IgG was added, and the sample incubated for another 2 h at room temperature. Radioactivity was counted after two washes of the pellets with saline. All positive sera were titrated, and results expressed as nanomoles of ^{125}I-MuSK precipitated per liter of serum.

Epitope mapping

Muscle-specific tyrosine kinase Ab-positive sera were tested by an RIA for the presence of IgG Abs to MuSK 1–2 or MuSK 3–4. In brief, 5 μl of each sample was incubated overnight at 4°C with ^{125}I-his-tag MuSK (40 000 cpm), ^{125}I-his-tag MuSK 1–2 (30 000 cpm), or ^{125}I-his-tag MuSK 3–4 (30 000 cpm), after which 50 μl of anti-human IgG was added. The samples then were incubated for another 2 h at room temperature. Radioactivity was counted after two washes of the pellets with saline.

IgG subclasses of MuSK Ab

Microtiter plates (Breakapart plate, Nunk-Immuno Module, Roskilde, Denmark) were coated with 100 μl of 10 μg/ml of each Ab to IgG subclasses (sheep polyclonal anti-human IgG1, 2, 3 and 4; Binding Site, Birmingham, UK) diluted with 10 mM sodium carbonate-bicarbonate buffer, pH 9.3 and kept for 1 h at room temperature. Nonspecific binding sites were saturated with 200 μl PBS containing 5% skimmed milk and 10% Blockace (Dainippon Seiyaku, Osaka, Japan) for 2 h at room temperature. A serum sample (20 μl), first incubated for 2 h at room temperature with ^{125}I-MuSK (30 000 cpm), was added to a plate, and the whole incubated for 2 h at room temperature. After four washes, ^{125}I was counted in each well.

Statistical analysis

Statistical analysis was performed by regression analysis, Kruskal–Wallis, one-way analysis of variance, and Student *t* test. A *P*-value of <0.05 was considered significant.

Results

MuSK Abs

The cut-off value (0.01 nM) was calculated from the mean + 3SD of the healthy subjects' values obtained by an RIA constructed with ^{125}I-MuSK extracellular domains. MuSK Ab was present in 23 (27%) of the 85 SNMG patients but not in any of the 272 SPMG patients, healthy subjects and patients with other neurological or immunological diseases (Fig. 1). Ab-positive samples were confirmed by serial dilution tests, and titers shown as nanomoles of ^{125}I-MuSK precipitated per liter of serum. MuSK Ab titers ranged from 8.4 to 240 nM (median, 57 nM). All the positive serum samples had extremely high titers on ^{125}I-human MuSK immunoprecipitation.

Clinical features of patients with MuSK Abs

Table 1 shows the clinical features of 23 MuSK Ab-positive patients. MuSK Ab in generalized SNMG showed female predominance (five men, 18 women) but not in ocular MG. Age at onset ranged from 18 to 72 years old (median 45 years). Clinical features of MuSK Ab-positive patients were confined to ocular [ptosis, 13/23 (57%) and double vision, 18/23 (78%)]; bulbar [dysphagia: 23/23 (100%), dysarthria: 19/23 (83%)]; neck extensor, 13/23 (57%); respiratory 8/23 (35%) muscle weaknesses. Prevailing weaknesses affected the oculobulbar and respiratory muscles of MuSK Ab-positive patients. About 48% (11/23) had no limb weakness. No thymomas were detected by CT. Six (26%) of the 23 MuSK Ab-positive patients who were thymectomized, had histological abnormalities including small hyperplastic features.

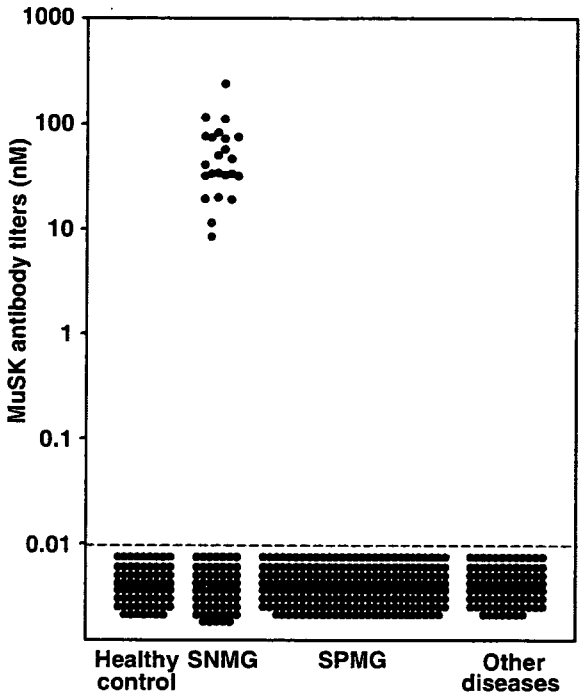

Figure 1 RIA-detected MuSK Ab titers of 85 patients with SNMG, 272 patients with SPMG, 91 patients with other neurological or immunological diseases, and 70 healthy participants. Broken line, the cutoff (0.01 nM) for MuSK Abs.

Table 1 Clinical features of MuSK Ab-positive patients

MuSK Ab positivity in SNMG	23/85 (27%)
MuSK Ab titers	8.4–239 (median 57 nM)
F:M	18:5
Age at onset	18–72 years (median 45 years)
Distribution of weakness	
Ptosis	13/23 (57%)
Ocular motor dysfunction	18/23 (78%)
Bulbar	23/23 (100%)
Neck	13/23 (57%)
Respiratory (crises)	8/23 (35%)
Limb	12/23 (52%)
Thymus	
Thymoma	0/23 (0%)
Hyperplasia	6/23 (26%)

Serial studies of clinical status and MuSK Abs

We measured MuSK Ab titer serially during the disease's course. Table 2 shows anti-MuSK Ab titers in relation to disease severity and duration, and immunosuppressive treatment (A), plasma exchange (B), or thymectomy (C). Disease severity was graded according to the Myasthenia Gravis Foundation of America (MGFA) classification [16] at the onset of myasthenic symptoms, in the maximally deteriorated state, and at

Table 2 Changes in MuSK Ab titers and in clinical status in MuSK Ab-positive patients

(A) Early steroid therapy

Case	Gender	Age at onset (years)	Duration (days)	MuSK Ab (nM)	MGFA classification	treatment
P-1	F	18	0	39.3	IIIb	
			56	39.0		Pred
			82	40.2		Pred
			138	38.0		Pred
			175	35.0	IIb	Pred
			313	33.0	PR	Pred
			577	21.0		Pred
P-2	F	32	0	113.0	IVb	Pred
			141	17.0		Pred
			261	15.0	IIb	Pred
			409	16.0		Pred
P-3	F	48	0	80.0	IVb	Pred
			46	28.0		Pred
			101	5.0		Pred
			1,641	4.2	PR	Pred
P-4	F	53	0	36.8	IIIb	
			41	31.0		Pred
			97	15.2		Pred
			111	10.0	IIb	Pred
P-5	F	52	0	240.0	V	Pred
			49	57.0		Pred
			77	22.9		Pred
			101	8.4		Pred
			129	3.0	IIb	Pred
P-6	F	76	0	33.0	IIb	Pred
			83	0.5		Pred
			118	0.2	PR	Pred

(B) Simple plasma exchange (PE)

P-7	M	53	0	74.4	V	
			42	59.0		
			52	47.0		
			PE ——→			
			62	28.5	IIb	
			PE ——→			
			67	17.2		
			125	16.0		Pred
			132	11.5		Pred
			138	9.0	IIb	Pred
P-8	M	71	0	113.9	IVb	
			PE ——→			
			11	32.1		
			45	32.0		Pred
			219	31.0		Pred
			616	28.0	IIb	Pred
P-9	F	66	0	30.0	IIIb	
			45	40.5		
			361	32.0		
			PE ——→			
			374	14.0	IIb	
			379	21.2		
			389	29.9		
			403	35.5	IIIb	Pred, Cyclo
			441	25.0		Pred, Cyclo
			476	20.5	IIb	Pred, Cyclo

Table 2 (Continued)

(C) Thymectomy (Tx)						
P-10	F	47	0	20.0		
			47	26.0	IIb	
			Tx ——→			
			95	47.2	IIIb	Pred
			270	19.8	IIb	Pred
P-11	F	52	0	22.6	IIb	
			58	23.2		
			Tx ——→			
			170	21.1		Pred
			255	25.0	IIb	
P-12	F	48	0	16.5	IIb	
			95	17.6		
			Tx ——→			
			210	15.7		Pred
			274	17.0	IIb	

PR, Pharmacological Remission; Pred, Predonisolone; Cyclo, Cyclosporine.

the last clinic visit after or during treatment. As shown in Table 2a, six patients (P1–P6) who underwent early steroid therapy showed impressive clinical improvement associated with a sharp decrease in anti-MuSK Ab titer; from 39.3 to 21.0 nM (P-1), 113.0 to 16.0 nM (P-2), 80.0 to 4.2 nM (P-3), 36.8 to 10.0 nM (P-4), 240.0 to 3.0 nM (P-5), and 33.0 to 0.2 nM (P-6). MG severities showed clinical improvement from class IIIb to pharmacological remission (PR) (P-1), class IVb to IIb (P-2), class IVb to PR (P-3), class IIIb to IIb (P-4), class V to IIb (P-5), and class IIb to PR (P-6).

Muscle-specific tyrosine kinase Ab titers of three patients were measured in serial samples taken before and after simple plasma exchange (Table 2b). The patients responded dramatically to that therapy, Ab titers decreasing from 74.4 to 9.0 nM (P-7), 113.9 to 28.0 nM (P-8), and from 30.0 to 20.5 nM (P-9), indicative of clinical improvement from class V to IIb (P-7), class IVb to IIb (P-8), and class IIIb to IIb (P-9). Moreover, conventional immunosuppression maintained the clinical improvement initially achieved by plasma exchange. In one patient (P-9), the effect had tapered off 45 days after plasma exchange, and Ab titer and disease severity returned to the level before treatment. Prednisolone and cyclosporin administered after MG relapse resulted in slower improvement.

Three patients who had histological abnormalities, including a small hyperplastic thymus, underwent thymectomies (Table 2c). After surgery one patient (P-10) immediately had worsening of dysphagia from class IIb to IIIb associated with a rapid increase in MuSK Ab titer from 26.0 to 47.2 nM. Thymectomy was not effective for the other two patients (P-11, P-12) who showed no change in disease severity and MuSK Ab titer.

We analyzed MuSK Ab titers in relation to quantitative clinical scores on the MGFA scale in serial studies of 12 individuals. MuSK Ab titers and disease severity were correlated ($P = 0.01$ by Kruskal–Wallis).

Epitopes in the extracellular domains of human MuSK

Eighteen sera with MuSK Abs were examined for ^{125}I-MuSK 1–2 and ^{125}I-MuSK 3–4 binding. All predominantly bound to ^{125}I-MuSK 1–2, range 68–97%. Only five of the 18 sera also showed slight binding (20–30%) to ^{125}I-MuSK 3–4 (Table 3).

IgG subclasses of MuSK Abs

In a solid phase RIA with sheep polyclonal antibodies to human IgG subclasses, in all the 18 sera tested MuSK Abs were exclusively IgG4 (Table 4).

Discussion

The MuSK Ab-positive rate found for generalized SNMG patients in Japan was 27% with female predominance (M:F = 5:18). This rate is lower than the 70% positivity originally reported [1] and the 40–50% recently reported [2–7]. It is consistent with the 27–33% reported for Japanese and Korean population [8–10] but significantly higher than the 3.8% Chinese positivity rate [11]. Age at onset ranged from 18 to 72 years old (median, 45 years); 61% of the patients presenting at >40 years of age, later than for Caucasians, and 57–71% of patients presenting at <40 years of age, but the differences was not significant [3,7,17,18].

Table 3 Ratio of MuSK Ig 1–2 and 3–4 Ab in MuSK 1–4 Ab titers

Case	MuSK Ab (nM)	Ig 1–2 domain (%)	Ig 3–4 domain(%)
1	8.4	97.1	2.9
2	19.3	68.1	31.9
3	32.5	81.2	18.8
4	50.0	82.7	17.3
5	33.4	97.3	2.7
6	31.8	95.7	4.3
7	19.9	91.0	9.0
8	11.4	95.2	4.8
9	40.7	87.9	12.1
10	32.0	91.0	9.0
11	33.6	95.0	5.0
12	74.7	95.4	4.6
13	72.0	76.2	23.8
14	46.2	80.8	19.2
15	74.7	96.9	3.1
16	82.2	74.2	25.8
17	110.7	89.5	10.5
18	114.6	71.2	28.8

Table 4 Ratio of IgG subclasses of MuSK Abs

Case	MuSK Ab (nM)	IgG 1 (%)	IgG 2 (%)	IgG 3 (%)	IgG 4 (%)
1	114.6	0.0	0.0	0.0	100.0
2	110.7	0.0	0.0	4.9	95.1
3	82.2	0.0	0.0	0.0	100.0
4	74.7	11.0	21.0	19.0	49.0
5	74.0	4.1	5.0	5.6	85.3
6	72.0	0.0	1.0	0.0	99.0
7	46.2	0.0	0.0	0.0	100.0
8	40.7	5.3	0.0	7.1	87.6
9	33.6	15.1	15.7	0.0	69.2
10	33.4	0.0	0.0	0.0	100.0
11	32.5	5.3	0.0	0.0	94.7
12	32.0	4.2	2.6	1.2	92.0
13	31.8	6.7	6.7	8.3	78.3
14	19.9	0.0	0.0	1.7	98.3
15	19.5	0.0	0.0	0.0	100.0
16	19.3	0.0	0.0	0.0	100.0
17	11.4	0.0	28.9	26.1	45.0
18	8.4	0.0	0.0	0.0	100.0

All the Ab-positive patients had similar patterns of muscle weakness, with prevalent involvement of the bulbar muscles in 100%, ocular symptoms (blepharoptosis and/or double vision) in 80%, and of the respiratory muscles in 35% with frequent myasthenic crises. Limb muscle involvement was comparatively less severe and inconsistent. Japanese MuSK Ab-positive patients therefore have clinical features similar in terms of the predominance of bulbar involvement to those reported for Caucasians.

We evaluated the correlation between MuSK Ab titers and disease severity. Table 2 shows patients who had a good response to early immunosuppressive therapy or simple plasma exchange. Their MuSK Ab titers sharply decreased in parallel with clinical improvement, whereas their Ab titers remained positive. We evaluated the effect of thymectomy in three individuals by measuring MuSK Ab titers in serum samples taken pre- and post-thymectomy. One patient's condition deteriorated after thymectomy and her Ab titer greatly increased. The two others showed neither progression nor Ab titer change during the observation period. Thymectomy therefore did not produce good results. Histological changes in the thymus of MuSK Ab-positive subjects are reported to be minimal and to include rare small germinal centers [19,20] in contrast to SPMG patients who had lymph node-type infiltrates. These findings, together with the lack of benefit of thymectomy, are evidence against a role for the thymus in antigen presentation and antibody production.

Serial studies showed a statistically close correlation between MuSK Ab titers and disease severity. MuSK Ab titers also recently were found to correlate with MG severity [21]. MuSK Ab titers were extremely high in all the positive cases (Fig. 1). The close relationship between clinical status and MuSK Ab, found by monitoring Ab titers, suggests that MuSK Ab has a significant pathogenic role in MG patients. Circulating MuSK Abs, however, are reported not to cause a MuSK or AChR deficiency at the endplates [22]. Recent experimental models (rabbits [13] and mice [23]), developed by immunization with recombinant MuSK ectodomain protein, produced MG-like muscle weakness with reduced AChR clustering at neuromuscular junctions. These findings clarified the pathogenic MG mechanisms produced by MuSK Ab.

The paramount MuSK Ab IgG subclass in our eighteen patients was IgG4. Limb and intercostal muscle biopsies found neither reduction in AChR numbers nor complement deposition [9,24]. The absence of complement deposits at a patient's end plates is explained by the fact that MuSK Ab is mainly IgG class 4 which does not fix complement [5,25]. The MuSK extracellular domain consists of four MuSK immunoglobulin-like (Ig) domains. Binding analysis of MuSK Abs to ^{125}I-MuSK Ig 1–2 or ^{125}I-MuSK Ig 3–4 showed that the eighteen sera tested predominantly bound to the ^{125}I-MuSK Ig 1–2 domain. The epitope was the N-terminal of the extracellular domain of human MuSK as described previously [5]. Furthermore, MuSK Abs have been shown to inhibit agrin-induced clustering of AChRs [26]. In fact, MuSK Ig 1–2 domains are more responsible for agrin responsiveness of MuSK, in contrast to Ig 3-4 domains which are more responsible for rapsyn association. We postulate that this is relevant to our findings of predominant binding analysis to MuSK Ig 1–2. The characteristics of the MuSK IgG subclass and Ab binding epitope in Japanese patients therefore are similar to those of Caucasians.

Muscle-specific tyrosine kinase Ab-positive patients often suffer facial and tongue muscle atrophy [3,27]. Benveniste *et al.*[28] reported that MuSK Ab plasma may affect the expression of atrophy-related protein and that a facial muscle, the masseter, is the most susceptible. Amongst our MuSK Ab-positive patients, four patients had detectable tongue atrophy from a relatively early phase of illness; weakness was moderate in 2 patients and mild in two patients. More *in vitro* and *in vivo* studies are needed to clarify the pathologic mechanisms that cause the muscle weakness produced by MuSK Ab. MuSK Ab detection provides a valuable biological means of support for the clinical diagnosis of MG and a way to monitor its clinical course.

Acknowledgements

This study was supported in part by a grant-in-aid from the Ministry of Education, Culture, Sports, Science and

Technology, Japan, and grants from the High-Tech Research Center, the Kobe Pharmaceutical University Collaboration Fund, and the Science Research Promotion Fund of the Japan Private School Promotion Foundation.

References

1. Hoch W, McConville J, Helms S, Newsom-Davis J, Melms A, Vincent A. Auto-antibodies to the receptor tyrosine kinase MuSK in patients with myasthenia gravis without acetylcholine receptor antibodies. *Nature Medicine* 2001; **7:** 365–368.
2. Vincent A, Bowen J, Newsom-Davis J, McConville J. Seronegative generalized myasthenia gravis: clinical features, antibodies, and their targets. *Lancet Neurology* 2003; **2:** 99–106.
3. Evoli A, Tonali PA, Padua L, *et al.* Clinical correlates with anti-MuSK antibodies in generalized seronegative myasthenia gravis. *Brain* 2003; **126:** 2304–2311.
4. Sanders DB, El-Salem K, Massey, JM, McConville J, Vincent A. Clinical aspects of MuSK antibody positive-seronegative MG. *Neurology* 2003; **60:** 1978–1980.
5. McConville J, Farrugia ME, Beeson D, *et al.* Detection and characterization of MuSK antibodies in seronegative Myasthenia gravis. *Annals of Neurology* 2004; **55:** 580–584.
6. Zhou L, McConville J, Chaudhry V, *et al.* Clinical comparison of muscle-specific tyrosine kinase (MuSK) antibody-positive and - negative myasthenic patients. *Muscle and Nerve* 2004; **30:** 55–60.
7. Padua L, Tonali P, Aprile I, *et al.* Seronegative myasthenia gravis: comparison of neurophysiological picture in MuSK+ and MuSK- patients. *European Journal of Neurology* 2006; **13:** 273–276.
8. Ohta K, Shigemoto K, Kubo S, *et al.* MuSK Ab described in seropositive MG sera found to be Ab to alkaline phosphatase. *Neurology* 2005; **65:** 1988.
9. Shiraishi H, Yoshimura T, Fukudome T, *et al.* Acetylcholine receptors loss and postsynaptic damage in MuSK antibody-positive myasthenia gravis. *Annals of Neurology* 2005; **57:** 289–293.
10. Lee JY, Sung JJ, Cho JY, *et al.* MuSK antibody-positive, seronegative myasthenia gravis in Korea. *Journal of Clinical Neuroscience* 2006; **13:** 353–355.
11. Yeh JH, Chen WH, Chiu HC, Vincent A. Low frequency of MuSK antibody in generalized seronegative myasthenia gravis among Chinese. *Neurology* 2004; **62:** 2131.
12. Chiu HC, de Lange GG, Willcox N, *et al.* Immunoglobulin allotypes in Caucasian and Chinese myasthenia gravis: differences from Japanese patients. *Journal of Neurology, Neurosurgery, and Psychiatry* 1988; **51:** 214–217.
13. Shigemoto K, Kubo S, Maruyama N, *et al.* Induction of myasthenia by immunization against muscle-specific kinase. *Journal of Clinical Investigation* 2006; **116:** 1016–1024.
14. Hopf C, Hoch W. Tyrosine phosphorylation of the muscle-specific kinase is exclusively induced by acetylcholine receptor-aggregation agrin fragments. *European Journal of Biochemistry* 1998; **253:** 382–389.
15. Hunter WM, Greenwood FC. Preparation of iodine-131 labeled human growth hormone of high specific activity. *Nature* 1962; **194:** 495–496.
16. Jaretzki A, Barohn RJ, Ernstoff RM, Kaminski HJ, Keesey JC, Penn AS. Myasthenia gravis: recommendations for clinical research standards. Task Force of the Medical Scientific Advisory Board of the Myasthenia Gravis Foundation of America. *Neurology* 2000; **55:** 16–23.
17. Lavrnic D, Losen M, Vujic A, *et al.* The features of myasthenia gravis with autoantibodies to MuSK. *Journal of Neurology, Neurosurgery, and Psychiatry* 2005; **76:** 1099–1102.
18. Diaz-Manera JA, Juarez C. Rojas-Garcia R, *et al.* Seronegative myasthenia gravis and antiMuSK positive antibodies: description of Spanish series. *Medicina Clinica (Barc)* 2005; **125:** 100–102.
19. Lauriola L, Ranelletti F, Maggiano N, *et al.* Thymus changes in anti-MuSK-positive and –negative myasthenia gravis. *Neurology* 2005; **64:** 536–538.
20. Leite MI, Strobel P, Jones M, *et al.* Fewer thymic changes in MuSK antibody-positive than in Musk antibody-negative MG. *Annals of Neurology* 2005; **57:** 444–448.
21. Bartoccioni E, Scuderi F, Minicuci GM, *et al.* Anti-Musk antibodies: correlation with myasthenia gravis severity. *Neurology* 2006; **67:** 505–507.
22. Selcen D, Fukuda T, Shen XM, Engel AG. Are MuSK antibodies the primary cause of myasthenic symptoms? *Neurology* 2004; **62:** 1945–1950.
23. Jha S, Xu K, Maruta T, *et al.* Myasthenia gravis induced in mice by immunization with the recombinant extracellular domain of rat muscle-specific kinase (MuSK). *Journal of Neuroimmunology* 2006; **175:** 107–117.
24. Vincent A, Leite MI. Neuromuscular junction autoimmune disease: muscle-specific kinase antibodies and treatments for myasthenia gravis. *Current Opinion in Neurology* 2005; **18:** 519–525.
25. Vincent A, Bowen J, Newsom-Davis J, McConville J. Seronegative generalized myasthenia gravis: clinical features and their targets. *Lancet Neurology* 2003; **2:** 99–106.
26. Farrugia ME, Bonifati DM, Clover L, Cossins J, Beeson D, Vincent A. Effect of sera from AChR-antibody negative myasthenia gravis patients on AChR and MuSK in cell cultures. *Journal of Neuroimmunology*, 2007; **185:** 136–144.
27. Farrugia ME, Robson MD, Clover L, *et al.* MRI and clinical studies of facial and bulbar muscle involvement in MuSK antibody-associated myasthenia gravis. *Brain* 2006; **129:** 1481–1492.
28. Benveniste O, Jacobson L, Farrugia ME, Clover L, Vincent A. MuSK antibody-positive myasthenia gravis plasma modifies MURF-1 expression in C2C12 cultures and mouse muscle in vivo. *Journal of Neuroimmunology* 2005; **170:** 41–48.

Acta Oto-Laryngologica, 2007; 127: 1024–1030

informa
healthcare

ORIGINAL ARTICLE

Quantitative analysis of mRNA in human temporal bones

YURIKA KIMURA[1,2,3], SACHIHO KUBO[2], HIROKO KODA[3], YOSHIHIRO NOGUCHI[3], MOTOJI SAWABE[4], NAOKI MARUYAMA[2] & KEN KITAMURA[3]

[1]*Departments of Otolaryngology and* [4]*Pathology, Tokyo Metropolitan Geriatric Hospital,* [2]*Aging Regulation Group, Research Team for Molecular Biomarkers, Tokyo Metropolitan Institute of Gerontolog and* [3]*Department of Otolaryngology, Graduate School, Tokyo Medical and Dental University, Tokyo, Japan*

Abstract

Conclusion. Well-preserved mRNA could be extracted from frozen human inner ears. Therefore, this study demonstrates that analysis of mRNA could be performed to study the molecular mechanisms of inner ear disorders using human specimens. *Objectives.* Analysis of RNA as well DNA is requisite to study the molecular mechanisms of inner ear disorders. Methods of isolating RNA from experimental animals have been established, while isolation of RNA from human inner ears is much more challenging. In the present study, we demonstrate a method by which messenger RNA (mRNA) was extracted from human inner ears and quantitatively analyzed. *Materials and methods. COCH* mRNA as well as *GAPDH* mRNA was extracted from membranous labyrinths dissected from three formalin-fixed and three frozen human temporal bones, removed at autopsy. The length of *COCH* mRNA and quantity of *GAPDH* mRNA was compared between the two groups by quantitative RT-PCR. *Results. COCH* mRNA could be amplified as much as 976 bp in all three frozen specimens. By contrast, it was amplified to 249 bp in two of the three formalin-fixed specimens, with no amplification observed in the remaining. The quantity of amplifiable *GAPDH* mRNA in the formalin specimens was only 1% of that of the frozen specimens.

Keywords: *Hearing loss, human, inner ear, mRNA, PCR*

Introduction

The mechanisms of sensorineural hearing loss have been analyzed with the recent advent of advanced molecular techniques. Studies of animals including mice have also contributed to identifying deafness genes and determining genotype–phenotype correlations [1,2]. In contrast, molecular analysis using human inner ear specimens is difficult because human inner ear specimens are inaccessible and formalin-fixed, celloidin-embedded temporal bone specimens are unsuitable for molecular analysis even though this method has been standard in histopathologic studies of the human temporal bones [3]. Nonetheless, there have been several reports in which DNA has been extracted from human inner ear specimens. Wackym et al. reported the first study using molecular biological techniques for human temporal bone pathology in 1993 [4]. They succeeded in amplifying mitochondria DNA by PCR and emphasized the difficulty of analyzing DNA from the human temporal bone because of the autolysis that occurs before fixation. They also reported PCR amplification of varicella-zoster virus DNA from temporal bone sections [5], as well as histopathologic analysis of a patient with Ramsay Hunt syndrome [6]. Moreover, the possibility of a relationship between presbycusis and a 4977 bp mtDNA deletion was suggested by PCR amplification of mtDNA from the cochlea of a celloidin-embedded human archival temporal bone [7]. We recently reported a quantitative analysis of mtDNA from a patient with a mutation at nucleotide 3243 [8] and detection of mitochondrial DNA from human inner ears using real-time PCR and laser microdissection [9] to elucidate mitochondrial hearing impairment. However, the availability of DNA analysis at a tissue level is limited to measurement of

Correspondence: Dr Ken Kitamura, Department of Otolaryngology, Tokyo Medical and Dental University, Graduate School, Yushima, Bunkyo-ku, Tokyo, 113-8519 Japan. Tel: +81 3 5803 5303. Fax: +81 3 5803 0146. E-mail: kitamura.oto@tmd.ac.jp

(Received 29 September 2006; accepted 14 December 2006)

ISSN 0001-6489 print/ISSN 1651-2551 online
DOI: 10.1080/00016480701200202

the heteroplasmy mutation ratio in mitochondrial hearing impairment or detection of a DNA virus, as mentioned above.

By contrast, analysis of mRNA expression patterns can demonstrate the spatio-temporal activities of gene transcription and expression in tissues, providing important physiological and pathological information at the molecular level [10]. Further, mRNA is important because it is a 'working copy' of a gene that directs biological activities of cells through the synthesis of proteins. Therefore, studying mRNA extracted from human inner ears can provide further information concerning the molecular mechanisms of inner ear disorders in humans. As removing temporal bones at autopsy is a regular method for studying human specimens, we analyzed and compared mRNA in formalin-fixed and frozen temporal bones removed at autopsy. The purpose of the present report was to establish the optimal method of extracting mRNA suitable for molecular biological applications from autopsied human temporal bones.

Materials and methods

Temporal bones

Six human temporal bones from five subjects with no hearing impairment (according to nursing records) were obtained at brain autopsy. Three were formalin-fixed and the others were put into the deep freezer as soon as possible after harvest and conserved by freezing at −80°C. The average age of the subjects was 77.0 years (range 72–83 years). The average time period between death and the start of autopsy was 20.1 h (range 4–47 h). Consent for using organs removed at autopsy was obtained from the patients' relatives. The present study was approved by the Ethical Review Board at Tokyo Metropolitan Geriatric Medical Hospital, pursuant to Article 18 of the Cadaver Autopsy and Preservation Act. Temporal bones were processed according to the surface preparation method (Figure 1) [11]. To avoid the degradation of RNA, we used RNAlater® (Ambion, Austin, TX, USA) to impregnate the temporal bone during the process and injected it into the inner ear from the oval window. The geniculate ganglion of facial nerves and the membranous labyrinth were dissected and immersed in a 1.5 ml microtube with 0.2 ml ISOGEN® (Nippon Gene, Tokyo, Japan).

Total RNA extraction and reverse transcription

Temporal bone samples were stored for an average of 7.5 months (range 2–18 months) before dissection. Dissected tissues were homogenized and mixed with 0.6 ml of ISOGEN®. After storage at room temperature for 5 min, 0.2 ml of chloroform was added. The mixture was shaken vigorously for 30 s, stored for 5 min at 4°C, and centrifuged at 15 000 g for 15 min at 4°C. The aqueous phase was transferred to microtubes, and 0.5 ml of chloroform was added. The mixture was shaken vigorously for 30 s, stored for 5 min at 4°C and centrifuged at 15 000 g for 15 min again. The supernatant was transferred and mixed with 0.5 µl of glycogen and 0.8 ml of isopropanol. After storage for >30 min at 4°C, the mixture was centrifuged at 15 000 g for 15 min at 4°C. The resultant supernatant was then carefully removed. The pellet containing RNA was washed with 70% ethanol three times, allowed to air-dry, and dissolved in 20 µl of RNase-free ddH_2O. The RNA concentration was determined by OD_{260}, measured by an ND-1000 Spectrophotometer® (NanoDrop, Wilmington, DE, USA). Approximately 40 ng of total RNA per sample was reverse transcripted in a 20 µl reaction using Transcriptor First Strand cDNA Synthesis Kit® (Roche, Basel, Switzerland) following the manufacturer's protocols.

PCR and sizing of PCR products

To compare the preserved length of mRNA between formalin-fixed and frozen samples, primers were designed using Primer 3 (http://frodo.wi.mit.edu/cgi-bin/primer3/primer3_www.cgi), on mRNA of *COCH* (accession no. NM004086), the coded protein of which is abundant in the inner ear [12]. Eight forward primers and one reverse primer were made to amplify 249–976 bp cDNA fragments (Figure 2). PCR was performed in a 20 µl volume containing 10 µl Premix Taq® (Takara Bio, Otsu, Japan), 0.5 µM of each specific primer and 1 µl of cDNA from the RT reaction. After initial incubation at 94°C for 3 min, the reaction mixtures were subjected to 35 cycles of amplification using the following sequence: 94°C for 30 s, 55°C for 30 s, and 72°C for 45 s. This was followed by a final extension step at 72°C for 7 min. Finally, 8 µl of the reaction mixture was run on a 2% agarose gel and visualized with ethidium bromide. Each amplification product was sequenced on an ABI PRISM® 3100 Genetic Analyzer (Applied Biosystems, Foster City, CA, USA).

Quantitative PCR analysis

To compare the quantity of mRNA for PCR level, quantitative real-time PCR was performed. TaqMan PCR® is a quantitative real-time PCR technique based on the 5′ exonuclease activity of TaqPolymerase [13]. In addition to the sense and antisense primers, a nonextendable oligonucleotide probe with

Figure 1. Temporal bones were processed according to the surface preparation method, and impregnated with RNAlater® (Ambion) to avoid the resolution of RNA. The membranous labyrinth was dissected. Arrows indicate pigmentation of stria vascularis.

a 5′ fluorescent reporter dye and a 3′ quencher dye were used. During the extension phase, Taq polymerase hydrolyzes the probe, thereby generating a fluorescent signal. In our experiment, this signal was monitored using 7300 Real-Time PCR System® (Applied Biosystems).

Primer name	Sequences	Product size
COCH-F1	TGATGACATCGAGGAAGCAG	249
COCH-F2	ACAGGAAAAGCCTTGAAGCA	356
COCH-F3	GCCAGTGAACATCCCAAAAT	461
COCH-F4	GCAGCGCCGATTTAATTTAC	555
COCH-F5	ACAAGCAGTGTCCACAGCAC	681
COCH-F6	GGCATCCAGTCTCAAATGCT	764
COCH-F7	TCCACAGGGGAGTAATCAGC	853
COCH-F8	GAGGCTTGGACATCAGGAAA	976
COCH-R	CAGGTCTTGCTGCACATCAT	

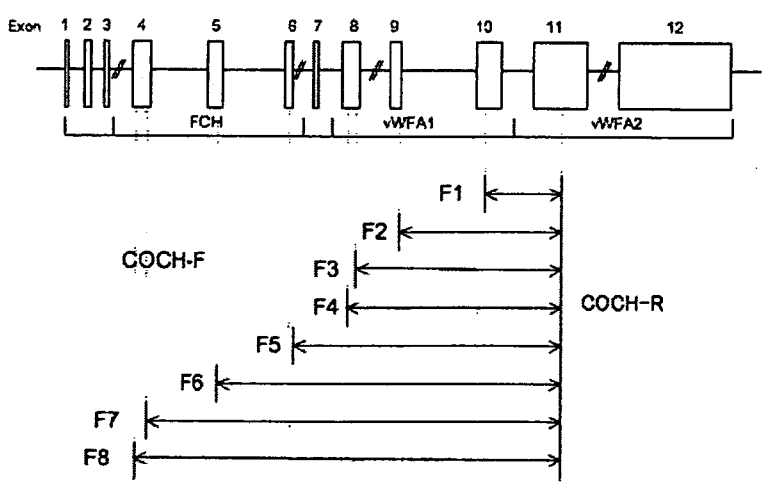

Figure 2. Primer sequences and amplified fragment size. Schematic drawing of the locus amplified by these primers in human *COCH* genomic structure. Exons are indicated by shaded boxes. The region of Limulus factor C homology (FCH) spans exon 4–6. The von Willebrand factor A-like domain, vWFA1, is contained in exon 8–10; vWA2 is in exon 11 and 12. Each primer set is in coding region.

We measured levels of *GAPDH*, which is a well-known housekeeping gene. PCR primers and probes were provided by TaqMan® GAPDH Control Reagents kit (ABI). PCR was performed in a 20 μl volume containing 10 μl Premix Ex Taq® (Takara Bio, Otsu, Japan), 0.2 μM of each specific primer, 0.1 μl of the GAPDH probe, 0.4 μl of Rox Reference Dye, and 1 μl of cDNA from the RT reaction. After initial incubation at 95°C for 10 s, the reaction mixtures were subjected to 45 cycles of amplification using the following sequence: 95°C for 5 s and 60°C for 31 s. This was followed by a final extension step: 95°C for 15 s, 60°C for 1 min and 95°C for 15 s. TaqMan PCR® was performed twice for each sample.

To quantify mRNA for PCR levels, we recorded the average number of PCR cycles (Ct) required for each reaction's fluorescence to cross a threshold value of intensity, set to pass through the linear portion of the amplification curve. Frozen samples were defined as standards, and the difference in Ct between the formalin-fixed samples and the standards was used to calculate dCt. The quantity relative to the standard was obtained from 2^{-dCt} [14]. The Student's t test was used for comparison between the two groups, and a probability value <0.05 was considered statistically significant.

Results

Total RNA yield

Average total RNA yield measured by ND-1000 Spectrophotometer® was 0.89 ± 0.40 μg of formalin-fixed samples and 2.73 ± 1.11 μg of frozen samples.

Comparison of the length of RT-PCR products for frozen and formalin-fixed samples

The results of the *COCH* mRNA RT-PCR amplification are shown in Figure 3a and b, in comparison to the RT-PCR product migration in the gel with the migration of a 50 bp ladder marker (lane 1). Lanes 2–9 show the results of the RT-PCR amplification using *COCH* primers. Amplification to 976 bp was possible in all three frozen samples. On the other hand, among the three formalin-fixed samples, two could be amplified to only 249 bp and the other could not be amplified with these primers. By sequencing the amplification product, these bands were confirmed as targeted locus.

Comparison of the quantity of real-time RT-PCR products between frozen and formalin-fixed specimens

The frozen samples were determined as standards, and the difference in Ct value between formalin-fixed samples and these standards was defined as

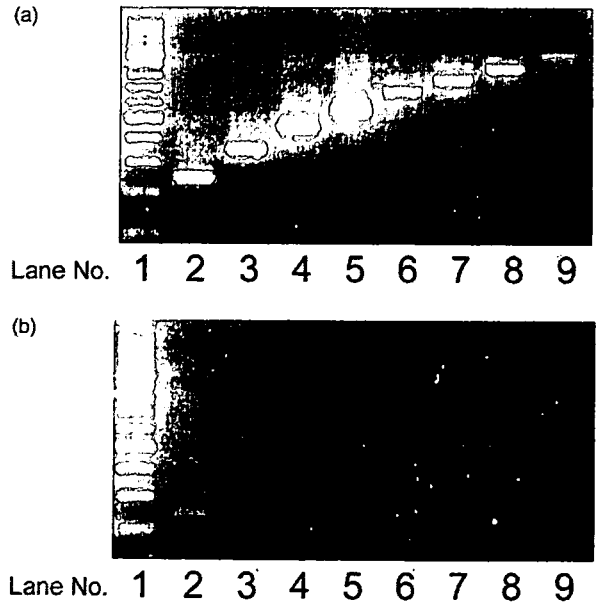

Figure 3. RT-PCR product migration in the gel with the migration of a 50 bp ladder marker (lane 1). Lanes 2–9 show the results of the RT-PCR amplification using *COCH* primers (a, frozen section; b, formalin-fixed sample). Amplification to 976 bp was possible in all three frozen samples; by contrast, two of the formalin-fixed samples could be amplified to only 249 bp and the other could not be amplified with these primers. Lane 2 shows a 249 bp fragment; lane 3, a 356 bp fragment; lane 4, 461 bp; lane 5, 555 bp; lane 6, 681 bp; lane 7, 764 bp; lane 853 bp; and lane 9, 976 bp.

Table I. Relative quantification using the comparative Ct method.

Conservation method	Average Ct	dCt (Ct − (Ct, frozen)	GADPH relative quantity to frozen sample
Frozen	27.37	0.00 ± 0.45	1.0 (0.7–1.4)
Formalin-fixation	33.65	−6.28 ± 0.56	0.012 (0.009–0.019)

The quantity of detectable GAPDH mRNA of frozen samples was defined as 1 while that of formalin-fixed samples was only 0.012.

dCt. As the efficiency of PCR is close to 1 according to Applied Biosystems guidelines, the value of 2^{-dCt} shows the mRNA quantity of PCR level relative to that of the standards. The average relative quantity of the *GAPDH* RT-PCR product is shown in Table I. There was a significant difference between the two groups. Only about 1% of the quantity of PCR product of the frozen samples was obtained using formalin-fixed samples.

Discussion

Analysis of inner ear function has progressed significantly from histological as well as molecular studies on experimental animals. In contrast, pathological study of the inner ear of humans with hearing loss is limited to cases in which brain autopsy is performed because it is impossible to access the inner ear during a patient's lifetime. Furthermore, the inner ear is present in hard bone tissue, and is highly differentiated anatomically and functionally. Therefore, it is difficult to study temporal bone molecular pathology by paraffin-embedded sections, nor can celloidin-embedded sections be relied upon [15].

To analyze real vital reactions at the molecular level, it is necessary to review manifestations of mRNA or protein. RT-PCR, in situ hybridization, Northern blot, or DNA microarrays for mRNA, and Western blot or immunostaining for protein are available for the analysis of vital reactions. However, these methods are usually difficult to apply to human inner ear specimens because these are usually formalin-fixed, celloidin-embedded specimens, which could easily degenerate and cause autolysis of fragile mRNA. Therefore, the human inner ear can be analyzed only for limited purposes. Lee et al. reported the first study of RT-PCR for archival temporal bones in 1997, in which they examined the manifestation of the γ-actin gene [16]. In this report, manifestation of γ-actin was detected in only 1 of 10 archival temporal bone specimens; the authors concluded that examination of the gene expression from an archival section was very limited because mRNA had been degraded by RNases. By contrast, Ohtani et al. reported that the α-tubulin gene was identifiable to 79% by nested RT-PCR in archival temporal bones in 1999 [17]. They concluded that the difference in their study from the former could be explained by the influence of primer design and RNA extraction methods. In formalin-fixed paraffin-embedded archival samples (liver tissue of mice), chemical modification such as methylol addition by formalin does not allow the direct application of extracted RNA to cDNA synthesis and RT-PCR [18].

In the present study, membranous labyrinths were dissected from three formalin-fixed and three frozen temporal bones and RNA was extracted from them. Then we compared the two samples based on how many base pairs of *COCH* mRNA were detectable. In addition, *GAPDH* mRNA was amplified by quantitative RT-PCR, and the quantities of RNA detectable by RT-PCR were compared. As a result, the *COCH* mRNA could be amplified to 976 bp in all the frozen sections, but among the formalin-fixed specimens, two could be amplified only to 249 bp while the other could not be amplified. In addition, the quantity of amplifiable *GAPDH* mRNA in the formalin-fixed specimens was only 1% of that of a frozen section. As a matter of course, both fragment lengths and quantities of RNA of formalin-fixed specimens are overwhelmingly smaller than those of frozen samples. Therefore, formalin-fixed temporal bone samples are not suitable for comprehensive molecular analysis, and conservation by freezing is desirable for introducing molecular pathological tools into human temporal bone pathology.

As for using autopsy specimens, Lin et al. reported RNA analysis of temporal bone soft tissues [10]. They collected temporal bones at immediate autopsies and showed manifestations and localizations of mRNA of mucin genes, such as MUC5B and MUC1, distributed in the submucosal gland of the eustachian tube and the middle ear, by Northern blot technique and in situ hybridization. They described how RNA degrades after death in a time-dependent manner, with the first obvious signs of degradation showing 6 h after death, and found mRNA was up to 1.4 kb in size at 6 h after death, indicating the preferability of an RNA analysis that uses molecular biological techniques within this time-frame.

However, in a regular clinical setting, it is not realistic to perform an autopsy within 6 h of death to obtain a temporal bone, not only from an ethical

perspective but also in terms of cooperation with a pathologist and the difficulty of processing specimens continuously. In our institution, removal of temporal bone specimens is included in the protocol of a conventional autopsy, and the average time from death to autopsy is 10 h. In this time, *COCH* mRNA could be amplified well up to 976 bp, which is the longest fragment expected by our primer planning. A continuous cryopreservation maneuver, which is routinely applied to preserve other organs, enables us to choose appropriate and effective analysis of precious cases. Therefore, our procedure is advantageous in that it can be performed in the protocol of a routine autopsy at any institution. Recently, Robertson et al. constructed a cDNA library from human fetuses at 16–22 weeks developmental age and reported that *COL1A2*, *COL2A2*, and *COL3A1*, which code types I, II, and III collagen, are intensely expressed by comparing expression levels with those of the brain by Northern blot technology [19]. They also reported that *COCH* emerged highly in the inner ear from the cDNA library, and these results led to the identification of *COCH* mutation causing DFNA9 [12,20,21]. Abe et al. extracted RNA from a cochlea obtained in an operation for acoustic neuroma or temporal bone tumor and reported that a strong manifestation of μ-crystallin (*CRYM*) in the membranous labyrinth was shown by the cDNA microarray method [22]. Furthermore, they suggested that *CRYM* mutation causes nonsyndromic deafness by *CRYM*.

In contrast to studies using human fetuses or surgical specimens, we studied autopsy specimens and succeeded in extracting mRNA in comparatively good condition. Using our proposed technique, the human inner ear can be studied by both molecular and histopathologic methods. Therefore, when human temporal bone specimens with almost the same hearing levels on both sides are obtained, we recommend that one side be formalin-fixed and celloidin-embedded and examined morphologically, while the other side be frozen and analyzed for mRNA or other molecules. Comparison of morphological and molecular biological examinations may elucidate pathologies of sensory neural hearing loss at the cellular and molecular level.

Conclusion

Well-preserved mRNA could be extracted from frozen human temporal bones removed at brain autopsy. The present study demonstrates that analysis of mRNA could be a clue in the study of molecular mechanisms of inner ear disorders using human temporal bones.

Acknowledgements

We would like to thank to Mr Kenichi Koizumi for excellent technical support, and Prof. Yukiko Iino and Prof. Yoshihiko Murakami for technical advice. This study was supported by 21st Century COE Program Brain Integration and Its Disorder[s] and a Grant-in-Aid for Scientific Research (nos 14770888, 15790924, 14370539, 17390457, 16659462, 16790 991, 17791163, 16012215, 18791194, 18791193) from the Ministry of Science, Education, Sports and Culture of Japan, and by Health and Labour Sciences Research Grants (H13-006; Research on Sensory and Communicative Disorders, and H14-21, H17-21 and no. 17242101; Research on Measures for Intractable Diseases) from the Ministry of Health, Labour and Welfare of Japan.

References

[1] Gibson F, Walsh J, Mburu P, Varela A, Brown KA, Antonio M, et al. A type VII myosin encoded by the mouse deafness gene shaker-1. Nature 1995;374:62–4.

[2] Everett LA, Belyantseva IA, Noben-Trauth K, Cantos R, Chen A, Thakkar SI, et al. Targeted disruption of mouse Pds provides insight about the inner-ear defects encountered in Pendred syndrome. Hum Mol Genet 2001;10:153–61.

[3] Schuknecht H. Pathology of the ear, 2nd edn. Philadelphia: Lea & Febiger; 1993.

[4] Wackym PA, Simpson TA, Gantz BJ, Smith RJ. Polymerase chain reaction amplification of DNA from archival celloidin-embedded human temporal bone sections. Laryngoscope 1993;103:583–9.

[5] Wacym PA, Popper P, Kerner MM, Grody WW. Varicella-zoster DNA in temporal bones of patients with Ramsay Hunt syndrome. Lancet 1993;342:1555.

[6] Wackym PA. Molecular temporal bone pathology: II. Ramsay Hunt syndrome (Herpes Zoster oticus). Laryngoscope 1997;107:1165–75.

[7] Seidman MD, Bai U, Khan MJ, Murphy MJ, Quirk WS, Castora FL, et al. Association of mitochondrial DNA deletions and cochlear pathology: a molecular biologic tool. Laryngoscope 1996;106:777–83.

[8] Takahashi K, Merchant SN, Miyazawa T, Yamaguchi T, McKenna MJ, Kouda H, et al. Temporal bone histopathological and quantitative analysis of mitochondrial DNA in MELAS. Laryngoscope 2003;113:1362–8.

[9] Kimura Y, Kouda H, Kobayashi D, Suzuki Y, Ishige I, Iino Y, et al. Detection of mitochondrial DNA from human inner ear using real-time polymerase chain reaction and laser microdissection. Acta Otolaryngol (Stockh) 2005;125:697–701.

[10] Lin J, Kawano H, Paparella MM, Ho SB. Improved RNA analysis for immediate autopsy of temporal bone soft tissues. Acta Otolaryngol (Stockh) 1999;119:787–95.

[11] Smith CA, Vernon JA. Handbook of auditory and vestibular research methods. Springfield, IL: Charles C Thomas; 1976. p. 5–51.

[12] Robertson NG, Skvorak AB, Yin Y, Weremowicz S, Johnson KR, Kovatch KA, et al. Mapping and characterization of a novel cochlear gene in human and in mouse: a positional candidate gene for a deafness disorder, DFNA9. Genomics 1997;15:345–54.